Radiation-induced defects in solid solutions and intermetallic compounds based on the Ni-Al system: II Recovery of radiation damage

1992 J. Phys.: Condens. Matter 4 10211

(http://iopscience.iop.org/0953-8984/4/50/010)

J. Phys.: Condens. Matter 4 (1992) 10211–10226. Printed in the UK

Radiation-induced defects in solid solutions and intermetallic compounds based on the Ni–Al system: II. Recovery of radiation damage

C Dimitrov†, B Sitaud†, X Zhang†, O Dimitrov†, U Dedek‡ and F Dworschak‡

† CECM–CNRS, 15 rue G Urbain, F94407 Vitry-sur-Seine Cedex, France
‡ IFF, KFA Jülich, PO Box 1913, D5170 Jülich, Federal Republic of Germany

Received 20 January 1992, in final form 21 August 1992

Abstract. The recovery of short-range-ordered Ni(Al) and Ni(Al,Ti) solid solutions and long-range-ordered Ni_3Al intermetallic compounds was investigated by residual electrical resistivity measurements as a function of composition and of fluence, after low-temperature (4–9 K) irradiation with 2.95 MeV electrons. In the solid solutions, long-range defect migration resulted in increases of local order; self-interstitials were found to be mobile above 110 K (at least in the binary alloys) and vacancies to be mobile above 330 K. The recovery spectrum of irradiated intermetallic compounds showed some similarity with that of pure nickel, with a smaller amount of fine structure. The mobility of self-interstitials (corresponding mainly to Ni–Ni dumbbells) occurs at a higher temperature (75 K) than in nickel (50 K) and does not induce significant ordering. By contrast, the Ni vacancies, which are the dominant vacancy species, are slightly less mobile than in nickel and promote some increase of long-range order.

1. Introduction

Several properties of nickel-based γ/γ' superalloys, which consist of a dispersion of an $L1_2$ long-range-ordered intermetallic compound in a nickel solid solution, are controlled by vacancy diffusion, both in the γ and in the γ' phase. This is the case for high-temperature creep, and for the long-term stability of the precipitate microstructure.

The present study aimed at determining the properties of point defects in a series of model materials based on the Ni–Al system, respectively representing the γ and γ' phases:

(i) Ni(Al) and Ni(Al,Ti) solid solutions;

(ii) Ni_3Al intermetallic compounds either stoichiometric or with Al concentrations above or below stoichiometry.

Low-temperature electron irradiations were used for introducing lattice defects, and the resulting damage was investigated by means of residual resistivity measurements. In a companion paper (paper I, Dimitrov *et al* 1992), damage production was reported and described in terms of defect production and of atomic order modifications. It was shown that damage rates, Frenkel-pair resistivities and recombination volumes in the solid solutions were comparable to those found in pure

0953-8984/92/5010211+16$07.50

nickel. In the Ni_3Al intermetallics, however, resistivity damage rates were larger by more than an order of magnitude. Although some disordering might occur during irradiation, it was concluded that defect production was the main contribution to the resistivity increase.

In the present paper, the recovery during isochronal anneals will be studied, for two initial defect concentrations, in order to determine the operative recovery mechanisms, and to obtain information on the mobilities of self-interstitials and vacancies.

2. Experimental details

The materials investigated were Ni/6 at.% Al, Ni/10 at.% Al, Ni/1 at.% Al/3 at.% Ti solid solutions (named $Ni_{94}Al_6$, $Ni_{90}Al_{10}Ni_{96}Al_1Ti_3$), three Ni_3Al intermetallic compounds containing 24.6, 25.0 and 26.5 at.% Al respectively (named $Ni_{75.4}Al_{24.6}$, $Ni_{75.0}Al_{25.0}$ and $Ni_{74.5}Al_{26.5}$), and pure nickel used as reference. The purity of the constituent elements, the preparation of the alloys and some data on their physical properties as well as specimen preparation and irradiation conditions have been reported in paper I (Dimitrov *et al* 1992). All materials were irradiated at two fluences, except $Ni_{96}Al_1Ti_3$ and $Ni_{75.4}Al_{24.6}$, which were irradiated only at one fluence. The radiation-induced excess resistivities $\Delta\rho_i$ and the fluences Φ are given in table 1.

The irradiated samples were isochronally pulse annealed *in situ* in the upper part of the cryostat for 15 min with temperature increments $\Delta T = 1$ K in the range 7–20 K, then $\Delta T = 0.03T$ up to 690 K. The recovery of the radiation damage was investigated by electrical resistivity determinations performed at 4.2 K. Resistivities were derived from the electrical resistances $\rho_{4.2\ K} = kR_{4.2\ K}$ by using the shape factors k determined before irradiation (Dimitrov *et al* 1992). A large uncertainty of ~ 25 nΩ cm was observed on the resistivity values of the Ni(Al) and Ni(Al,Ti) alloys. This was attributed to magnetostriction effects induced by the translation of the holder from the annealing position, in the furnace, to the helium bath, where resistance measurements were carried out. For the isochronal anneals above 100 K, the uncertainty was greatly reduced (to ~ 1 nΩ cm) by measuring the electrical resistances in a saturating longitudinal magnetic field H of 0.22 T. However, the resistivities $\rho_{H\neq 0}$ determined in these conditions were systematically larger, by a constant amount, than the $\rho_{H=0}$ ones. Therefore, at the end of the isochronal treatments carried out above 100 K, the electrical resistances were successively measured without and with a 0.22 T magnetic field. In order to obtain a homogeneous set of resistivity data in the whole range of annealing temperatures, the resistivity values were normalized to $\rho_{H=0}$ between 100 and 670 K by subtracting the effect of the magnetic field. In addition, the recovery curves of the solid solutions were smoothed in two temperature ranges: (i) up to 100 K, since the uncertainty on the electrical resistances, measured without a magnetic field, was large; (ii) in the range 100–250 K, where the resistivity variations, determined in the presence of a magnetic field, were comparable to the uncertainty of the measurements. No magnetostriction effects were detected in the nickel and intermetallic samples; consequently, the recovery curves were directly derived from the electrical resistance values measured without a magnetic field: the uncertainty of the corresponding resistivity determinations was ~ 4 nΩ cm.

Table 1. Composition and radiation-induced resistivity variations ($\Delta\rho_i$) in alloys irradiated to different fluences Φ.

	Al (at.%)	0	6	10	1 + 3Ti	24.6	25.0	26.5
$\Delta\rho$	$\Phi_1 = 4.3 \times 10^{18}$ e cm^{-2}	84	84[a]	102[a]	115[a]		1245	1521
(nΩ cm)	$\Phi_2 = 8.0 \times 10^{18}$ e cm^{-2}	160	154	195		2603	2369	2282

[a] $\Phi_1 = 4.2 \times 10^{18}$ e cm^{-2}.

3. Experimental results and discussion

In the electron-irradiated nickel samples, the isochronal resistivity recovery and the corresponding derivative curves (figure 1) agreed with the previous data obtained by Knöll *et al* (1974) and Bartels *et al* (1986, 1987b). The main features of the recovery are the following:

(i) Stage I (4.2–67 K) includes several substages; the main one, with a maximum recovery rate at 50 K, is associated with the correlated and uncorrelated recombination of interstitials with vacancies.

(ii) Stage II displays a fine structure in a broad temperature range (67–310 K) and is attributed to the growth or structure rearrangement of the small interstitial clusters formed at the end of stage I.

(iii) Stage III, appearing as a small peak centred at ~ 360 K, is identified with the migration of vacancies, according to positron annihilation data (Nguy 1988). At higher temperatures, recovery rate becomes very weak.

Our results on solid solutions and on intermetallic compounds will be discussed, in the next sections, with reference to the data of pure nickel irradiated in the same runs as the alloys.

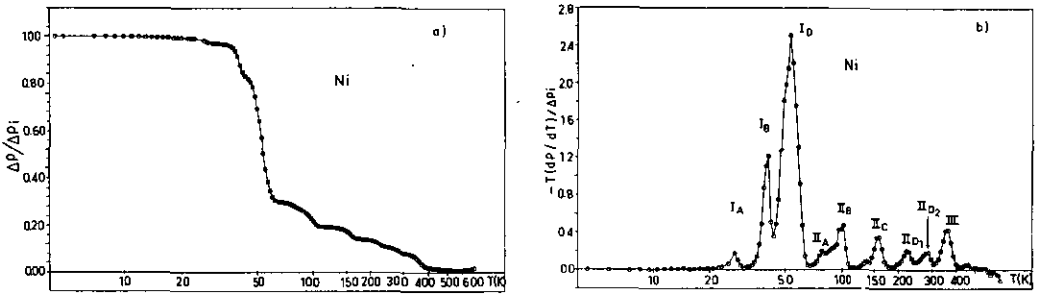

Figure 1. Isochronal resistivity recovery (*a*) and its logarithmic derivative (*b*) of pure Ni after 2.95 MeV electron irradiation to a fluence of 8.0×10^{18} e cm^{-2}.

3.1. Isochronal recovery of Ni(Al) and Ni(Al,Ti) alloys

3.1.1. General features of recovery curves. The resistivity variations observed in the solid solutions during isochronal annealing after electron irradiation are presented and described by considering both the effects of alloy composition and the influence of the initial defect concentrations.

(i) *Composition dependence.* The normalized variations of residual resistivity during the isochronal treatment, and their logarithmic derivatives, are presented on figure 2 as a function of temperature for the three alloys $Ni_{94}Al_6$, $Ni_{90}Al_{10}$, $Ni_{96}Al_1Ti_3$, irradiated to the same fluence, 4.2×10^{18} e cm^{-2}. The term $\Delta\rho_i$ corresponds to the increase of resistivity obtained at the end of the irradiation (table 1) and $\Delta\rho$ to the excess resistivity remaining after annealing at temperature T. All these curves have been obtained by applying the analysis method described in section 2, including the correction of the magnetic field. The general behaviour of the recovery points to the existence of four distinct temperature ranges.

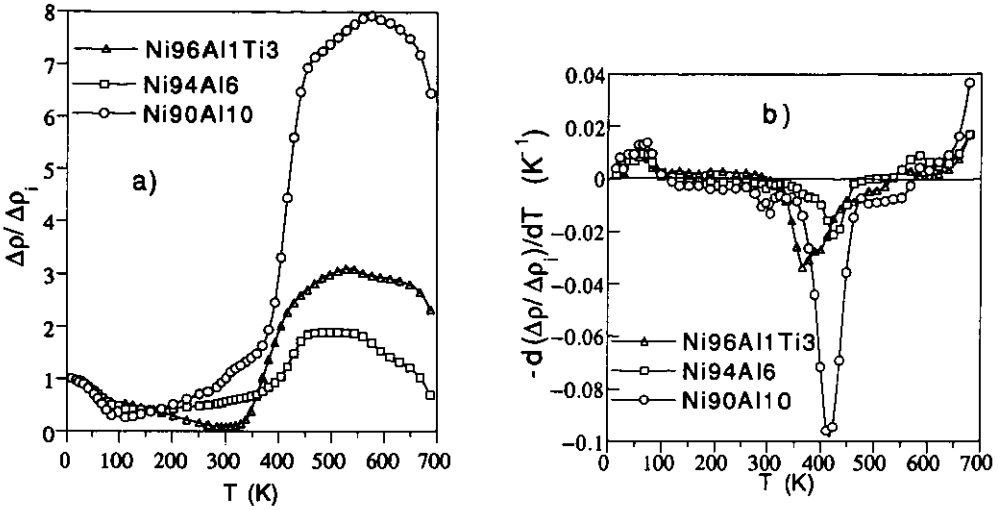

Figure 2. Isochronal resistivity recovery (*a*) and derivative curves (*b*) of the solid solutions electron irradiated to the same fluence (4.2×10^{18} e cm^{-2}).

Stage I: From 5 to ~ 110 K, the excess resistivity is reduced to a fraction (40–70%) of the initial value, according to the composition of the alloy.

Stage II: Between 110 and ~ 330 K, the recovery rates are nearly constant (figure 2(*b*)), with negative, zero or positive values.

Stage III: From 330 to 470 K, in all samples, very large resistivity increases are observed. The composition of the alloys clearly affects the relative amplitude of the variations, which can reach 600% of $\Delta\rho_i$ in $Ni_{90}Al_{10}$.

Stage IV: At higher temperatures, before a strong decrease, the resistivity values remain stable in the $Ni_{94}Al_6$ alloy or go through a maximum for the two other studied alloys.

Table 2. Temperature T_M of maximum recovery rate, absolute amplitude $\Delta\rho$ and relative amplitude $\Delta\rho/\Delta\rho_i$ of resistivity variations in the first three temperature ranges of isochronal recovery, in $NiAl_6$, $NiAl_{10}$ and $NiAl_1Ti_3$ alloys irradiated to 4.2×10^{18} e cm^{-2}.

	Stage I 5–110 K			Stage II 110–330 K		Stage III 330–470 K		
Alloys	T_M (K)	$\Delta\rho$ (nΩ cm)	$\Delta\rho/\Delta\rho_i$ (%)	$\Delta\rho$ (nΩ cm)	$\Delta\rho/\Delta\rho_i$ (%)	T_M (K)	$\Delta\rho$ (nΩ cm)	$\Delta\rho/\Delta\rho_i$ (%)
$NiAl_1Ti_3$	56	−50	−43	−40	−35	367	+280	+243
$NiAl_6$	59	−53	−63	+20	+24	426	+112	+133
$NiAl_{10}$	65	−73	−72	+98	+96	417	+583	+572

The main characteristics of the first three stages are summarized in table 2. The temperature of maximum recovery rate T_M of the first stage (stage I) appears to be nearly the same within ±5 K for the different alloys. Because of the lack of measurement accuracy in this part of the experiments, the small variation of T_M with the increase of solute concentration cannot be considered as significant. On the other hand, the temperature that characterizes stage III seems to be significantly lower in

the ternary alloy (367 K, as compared to 426 K and 417 K in the $Ni_{94}Al_6$ and $Ni_{90}Al_{10}$ binary solid solutions respectively).

(ii) *Fluence dependence.* Resistivity variations during isochronal anneals and the corresponding derivative curves are shown in figure 3, in the $Ni_{90}Al_{10}$ alloy, electron-irradiated at two different fluences. The general recovery behaviour described for the lower fluence (4.2×10^{18} e cm^{-2}) is unchanged when the initial defect concentration is multiplied by 2. The temperature of stage I is nearly the same in the two cases. By contrast, the increase of radiation fluence shifts the maximum of the recovery rate of stage III, from 417 K for 4.2×10^{18} to 407 K for 8.0×10^{18} e cm^{-2}. The amplitude of this stage depends slightly on the initial defect concentration. At higher temperatures (470–690 K), the resistivity variations are similar and the difference between the two curves corresponds to the one existing at the end of stage III.

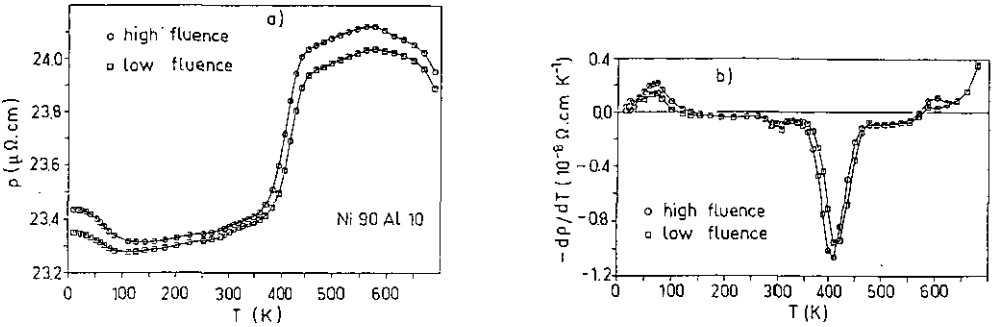

Figure 3. Resistivity changes as a function of annealing temperature (*a*) and derivative curves (*b*) of the $Ni_{90}Al_{10}$ solid solution electron irradiated at two fluences: 4.2×10^{18} and 8×10^{18} e cm^{-2}.

3.1.2. Qualitative interpretation of the different recovery stages. The recovery stages in these solid solutions can be explained by the contribution of two mechanisms, which have opposite effects on the resistivity variations. The first one involves defect annihilations, which take place in the same way as in pure nickel and result in resistivity decreases. The second one is due to short-range order (SRO) changes induced by the migration of defects. The evolution of SRO in the presence of thermal vacancies has been extensively investigated during isochronal, isothermal and cross-over experiments by resistivity measurements in the same alloys (Sitaud *et al* 1990), and a SRO increase was found to produce always an increase in residual resistivity.

In the first temperature range (stage I, 5–110 K), the resistivity decreases can be interpreted as the annihilation of Frenkel defects by close-pair recombinations without a significant variation of the degree of order of the alloys. Owing to the low measurement accuracy and probably also the several defect structures resulting from the presence of the different chemical species, no substages similar to those observed in pure nickel were detected. This lack of fine structure in the first recovery stage agrees with the results obtained in other concentrated solid solutions, like electron-irradiated Au–Ag (Bartels *et al* 1987a) and Fe–Cr–Ni alloys after neutron or electron irradiations (Dimitrov *et al* 1981, 1987). According to the suggestions made by these authors, the continuous shape of the recovery peak in the first stage can be explained

by the existence of a broad configuration-energy spectrum correlated with defect–solute atom interactions depending on the chemical environment of the individual defects.

The second stage (II, 110–330 K) exhibits a behaviour specific to each investigated alloy (figure 2). In the binary solid solutions, the increase of the Al concentration leads to an increase of the positive resistivity variation rate. Considering that in this temperature range the observed variations could result both from defect annihilation and from an SRO increase, one has to conclude that these two contributions are nearly equal in the $Ni_{94}Al_6$ alloy and that the SRO contribution is significantly more important in $Ni_{90}Al_{10}$. By contrast, the resistivity decrease observed in the ternary alloy suggests that the contribution of the defect annihilation is dominant: at 330 K the recovery is near 80%. Since ordering effects are important in this alloy (see the large variations observed in the next stage), such a decrease should result either from a small number of migration jumps of the defects in stage II, or from a low efficiency of these defects for promoting local order evolutions.

The positive variations observed in stage II for the Ni(Al) solid solutions can only be due to ordering effects, which require the long-range migration of defects exchanging with the different atomic species. Considering that in this temperature range vacancies are not mobile, as shown by positron annihilation experiments (Sitaud 1991), the defects involved in this process must be interstitials. The migration properties of interstitial defects in dilute FCC alloys have been treated by Dederichs *et al* (1978) on the basis of a theoretical application of empirical interatomic potentials. Their analysis shows that the stable structure of the interstitial depends strongly on the size of the solute as compared to that of the solvent. For atoms with a negative size effect, the solute becomes included in a ⟨100⟩ mixed dumbbell, which may subsequently migrate with or without dissociation according to the binding energy of the complex. For solutes with a positive size effect, the more stable configuration of the defect is a ⟨100⟩ pure dumbbell localized on a nearest-neighbour site of the solute atom. The migration of the split interstitial is then directly controlled by the solute trapping. In the following, we shall assume that the results of Dederichs' calculations are also valid in the present more concentrated alloys. The sign of the size effect can be determined from the crystal parameter variations resulting from the substitution of solvent atoms by solute atoms. From x-ray diffraction measurements it has been found, for the investigated concentrations in Ni(Al) and Ni(Al,Ti) alloys, that the size effect of the solutes was always positive. Owing to the alloy compositions ($C_{solute} \ll C_{Ni}$), the Ni–Ni split interstitial should be the dominant species on a purely statistical basis; this predominance is further increased by the lower configuration energy of this defect (see above). Nevertheless, the observed resistivity variations in the Ni(Al) alloys, which have been attributed to SRO evolutions, require at least a transient formation of Ni–Al mixed defects. In the ternary alloy, the dominant solute is titanium, which has, in nickel, a larger size effect than aluminium. Therefore the Ni–Ti mixed dumbbell might have a too large configuration energy to be formed by a thermally activated process in stage II. Thus in the $Ni_{96}Al_1Ti_3$ solid solution, only Ni–Ni interstitials could migrate without changing the state of short-range order: the resistivity variations are mainly due to defect annihilation and are therefore negative.

The next stage (III, 330–470 K) is characterized by a large resistivity increase caused by an enhancement of SRO and is assigned to vacancy migration in the solid solutions. This interpretation is supported by recent positron annihilation experiments performed on the same alloys during isochronal annealing after electron

irradiation (Sitaud 1991). This stage can be compared to stage III in pure nickel. The temperatures of maximum variation rate are slightly higher in the solid solutions than in nickel (table 2); however, in the two types of materials, resistivity evolutions are mainly caused by two different phenomena, the loss of vacancies in the pure metal and the short-range ordering by effective vacancy jumps in the alloys. This remark suggests that the use of stage temperatures for obtaining information about the activation enthalpy of vacancy migration is only significant if a comparison is made between different alloys. Considering that, for a given recovery mechanism, stage temperature is proportional to the activation enthalpy, the present data (table 2) show that the vacancy migration enthalpies are nearly equal in the $Ni_{94}Al_6$ and $Ni_{90}Al_{10}$ alloys and somewhat lower (by a factor 0.85) in the $Ni_{96}Al_1Ti_3$ alloy.

Finally, in stage IV all curves show a slowing down of the evolution before displaying a sharp decrease of resistivity above 600 K. This behaviour suggests that in the range 425–600 K the ordering effect vanishes because of a lack of mobile vacancies and also because the materials are near to their equilibrium state. In order to examine this effect, and to interpret the differences observed between the alloys, the resistivity evolutions during the isochronal annealing are displayed in figure 4 as a function of temperature, together with equilibrium resistivity values (broken curves). Equilibrium SRO resistivities were determined by extrapolating the experimental results obtained from thermal experiments on the same alloys, in which only thermal vacancies were present (Sitaud and Dimitrov 1989, 1990). In the $Ni_{96}Al_1Ti_3$ alloy, the resistivity increases continuously up to 525 K, which corresponds to the maximum of the total variation. This maximum may correspond to the thermodynamic equilibrium resistivity of this alloy, since it is located on the equilibrium curve. The subsequent decrease corresponds to thermal disordering; however, the atomic mobility remains too weak with respect to the annealing time to allow a structural evolution along equilibrium states. In the $Ni_{94}Al_6$ alloy, after the strong resistivity increase, a plateau is recorded between 450 and 550 K. The temperature at which the recovery curve of the irradiated sample crosses the thermal equilibrium curve corresponds to the end of stage III. The irradiation treatment thus allows the atomic order to reach an equilibrium state at a low temperature, $\sim$ 450 K, which could not be obtained directly by simple thermal treatments. The flat shape of the recovery isochronal curve beyond the temperature of curve crossing can be explained by a lack of atomic mobility directly correlated to the stability of vacancy clusters in this temperature range. For the $Ni_{90}Al_{10}$ alloy the resistivity goes through a maximum and begins to decrease before having reached the equilibrium curve. This observation shows that the position of the maximum is not always determined by a local order equilibrium but may correspond to a kinetic effect resulting from at least two processes with opposite contributions to the resistivity variations (for instance, an order resistivity including contributions of first- and second-neighbour SRO parameters). Such an explanation was also proposed, in the same alloy, to interpret the large 'cross-over' effect clearly demonstrated by Sitaud and Dimitrov (1990), in a kinetic study of order changes during thermal treatments.

3.2. Ni_3Al intermetallic compounds

3.2.1. General features of recovery curves. The resistivity recovery curves of the three Ni_3Al compounds are shown in figure 5(*a*) on a logarithmic temperature scale. The general behaviour is comparable to that determined in pure nickel: two main recovery stages are observed, but the ratio of their amplitudes is different from that of Ni. In nickel, stage I is much larger than stage III, whereas in Ni_3Al the opposite is observed.

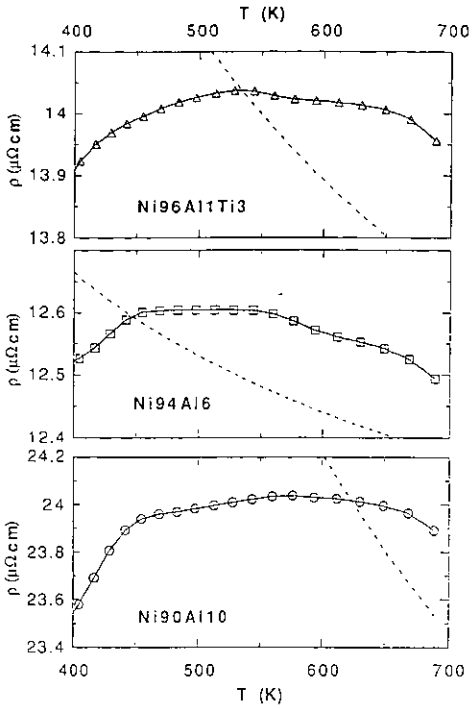

Figure 4. Resistivity changes above 400 K in the three solid solutions irradiated at the lower fluence, 4.2×10^{18} e cm^{-2} (open symbols), and equilibrium order resistivity curves (broken curves) determined in unirradiated samples (Sitaud and Dimitrov 1990).

Furthermore, an over-recovery appears, at ~ 600 K in the hyperstoichiometric alloy (26.5 at.% Al) and at lower temperatures in the other materials. This over-recovery, characterized by the total normalized recovery (last column in table 3(*b*)), depends on composition and on initial defect concentration. It is maximum at stoichiometry and decreases when deviation from stoichiometry increases, in samples irradiated at 8×10^{18} e cm^{-2}. Its relative amplitude increases when the initial defect concentration becomes smaller (figure 6).

The logarithmic derivative curves of the resistivity variations, relative to the alloys irradiated at the higher fluence (figure 5(*b*)), show the fine structure of the recovery spectrum. Similar spectra were observed for the lower fluence, with no significant appearance of a finer structure of the recovery stages (figure 8). The stages were labelled I, II, III and III′. Their relative amplitude and the temperature of maximum recovery rate are listed in table 3; the composition and fluence dependence are shown in figures 6 and 7.

3.2.2. Composition dependence of recovery stages. Stage I extends up to ~ 128 K. This first main recovery stage (47–32% of the radiation-induced resistivity) is characterized (figure 5(*b*)) by a peak at 75 K with shoulders on the high- and low-temperature sides. The temperature of maximum recovery rate appears to be independent of composition, although the shape of the peak varies and the relative amplitude of this stage decreases strongly with increasing aluminium content.

Stage II (128–292 K) represents 13–16% of the excess resistivity. The small peaks, corresponding probably to different substages, seem to be smoothed out and form a broad hump in the hyperstoichiometric compound (26.5 at.% Al).

Stage III (292–475 K) is the second main recovery stage (40–47% of the radiation-induced resistivity). Its temperature is composition dependent, the corresponding

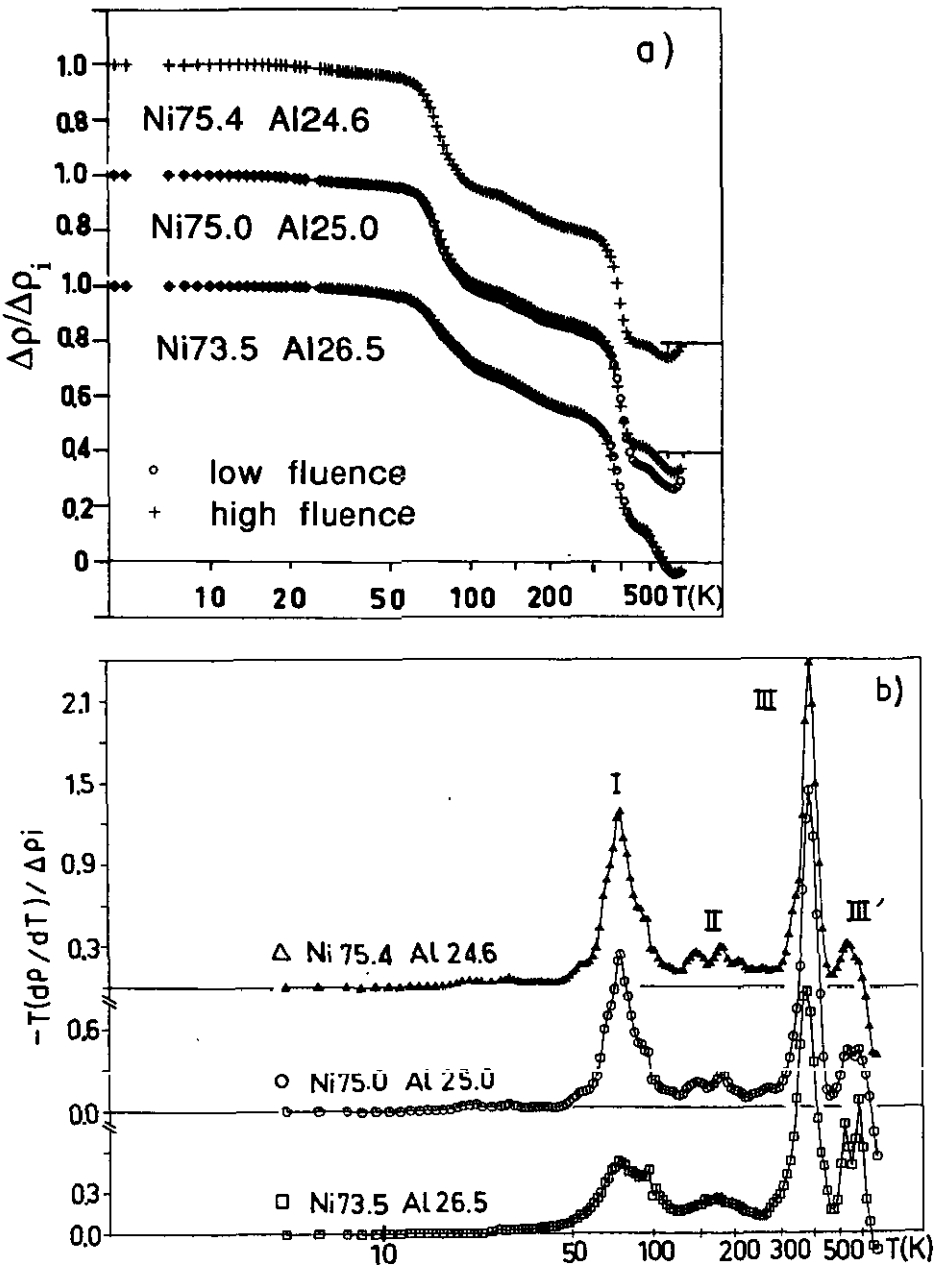

Figure 5. (*a*) Isochronal resistivity recovery of stoichiometric and off-stoichiometric Ni_3Al irradiated at two fluences, 8.0×10^{18} e cm^{-2} (Δ) and 4.3×10^{18} e cm^{-2} (○). (*b*) Logarithmic derivative curves of the same compounds irradiated at the higher fluence.

peak being shifted to lower temperatures by 15 K when the aluminium content increases; however its amplitude is maximum at stoichiometry and decreases slightly when composition deviates from stoichiometry.

A stage III′ is observed at higher temperatures, between 475 and 600 K. In the stoichiometric and hyperstoichiometric alloys, it is split into two substages, labelled

Table 3. (*a*) Temperatures T_M (K) of maximum recovery rate in the different stages of Ni_3Al compounds irradiated at fluence Φ. (*b*) Relative amplitudes of the recovery stages, $\Delta\rho/\Delta\rho_i$ (%).

(*a*) T_M (K).

Alloys	Φ (10^{18} e cm^{-2})	I	II_A	II_B	II_C	III	III'_1	III'_2
$Ni_{75.4}Al_{24.6}$	8.0	75.0	144.5	180.3	207.9	387.4	537.0	
$Ni_{75.0}Al_{25.0}$	4.3	74.9	145.3	180.4		397.3	544.5	
	8.0	74.9	145.2	180.1		384.8	537.2	581.8
$Ni_{73.5}Al_{26.5}$	4.3	74.7		172.7		387.9	525.9	580.0
	8.0	74.5		173.2		372.0	521.5	584.0

(*b*) $\Delta\rho/\Delta\rho_i$ (%).

Alloys	Φ (10^{18} e cm^{-2})	I 7–128 K	II 128–292 K	III 292–475 K	III′ 475–649 K	Total
$Ni_{75.4}Al_{24.6}$	8.0	47.1	14.1	40.2	4.8	106.2
$Ni_{75.0}Al_{25.0}$	4.3	44.7	13.3	47.7	8.5	114.2
	8.0	42.1	13.7	42.7	9.6	108.1
$Ni_{73.5}Al_{26.5}$	4.3	33.8	14.9	40.5	15.6	104.8
	8.0	32.1	16.1	40.0	15.8	104.0

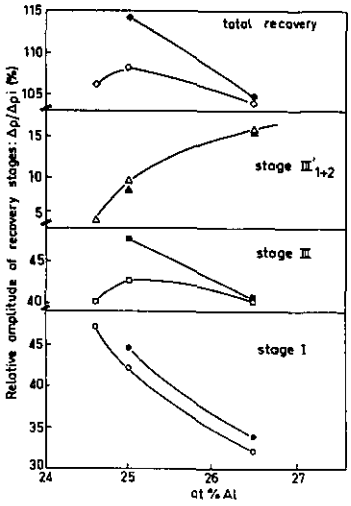

Figure 6. Fluence and composition dependence of the relative amplitude of recovery stages in electron-irradiated Ni_3Al (open symbols, higher fluence; full symbols, lower fluence).

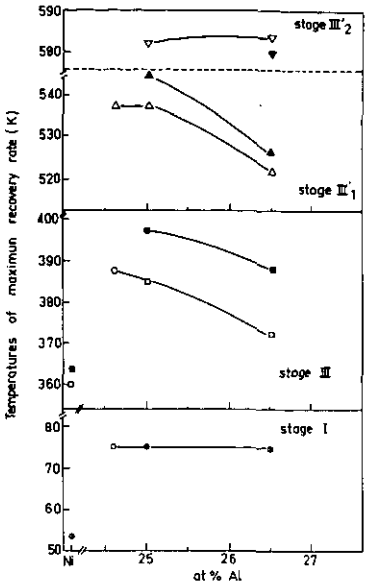

Figure 7. Fluence and composition dependence of the temperature of maximum recovery rates on the derivative curves of electron-irradiated Ni_3Al alloys (same symbols as in figure 6).

III'_1 and III'_2. (The second one appears as a shoulder on the high-temperature side of III'_1 in the hypostoichiometric alloy containing 24.6 at.% Al). An increasing Al content modifies stage III':

(i) its total amplitude grows,

(ii) substage III'_1 is shifted to lower temperatures, while it is slightly enhanced,

(iii) the temperature of substage III'_2 seems independent of composition, but the corresponding resistivity recovery increases.

3.2.3. Fluence dependence of recovery. The effect of initial defect concentration on the recovery was only studied in the stoichiometric and hyperstoichiometric (26.5 at.% Al) alloys. A decrease of defect concentration (lower fluence) leads to the following changes (table 3):

(i) The temperature of maximum recovery rate of stage I is unchanged; however, its relative amplitude increases.

(ii) Stage III is shifted to higher temperatures and its magnitude is particularly enhanced at stoichiometry.

(iii) Substage III'_1 is shifted to higher temperatures while substage III'_2 is rejected at lower temperatures (figure 7); at stoichiometry it merges with substage III'_1 (figure 8).

3.2.4. Configuration of point defects in Ni_3Al. From the discussion developed in paper I (Dimitrov *et al* 1992), the production of point defects (vacancies and self-interstitials) was concluded to be the dominant process in radiation damage. In order to contribute to the interpretation of the recovery spectrum, we discuss in this section some aspects of the expected defect configurations in the $L1_2$ structure of Ni_3Al.

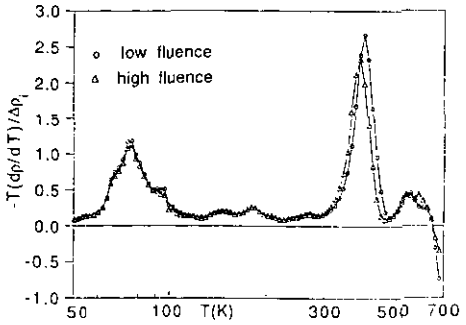

Figure 8. Derivative isochronal recovery curves of the stoichiometric Ni_3Al alloy electron irradiated to fluences of 8.0×10^{18} e cm^{-2}(Δ) and 4.3×10^{18} e cm^{-2}(O).

Assuming a vacancy defect to consist of an empty lattice site, two types of vacancies should exist in Ni_3Al according to their position on the Ni or Al sublattices; they will be designated as Ni and Al vacancies respectively.

Concerning the configuration of self-interstitials, it seems reasonable to assume that these defects are ⟨100⟩ dumbbell split interstitials by analogy with FCC nickel. This structure was found to be consistent with the results of x-ray diffuse scattering in irradiated $L1_2$ Ni_3Fe (Bender and Ehrhart 1982) and with the formation energy calculations of Caro *et al* (1990); it was also assumed in the case of Cu_3Au (Alamo *et al* 1986). Three types of dumbbells can be produced with different probabilities by irradiation: Ni–Ni (on Ni sites), Ni–Al mixed dumbbells (distributed on both Ni and Al sites) and Al–Al (on Al sites).

On the basis of the environment of Ni–Ni dumbbells (four Al and eight Ni atoms as nearest neighbours), we have to consider two orientations for these defects, characterized by different configuration energies. The minority A-type Ni–Ni dumbbells have their axis along the intersection of two {100} planes of the Ni sublattice. They are stabilized by the attractive binding energy of the four oversized nearest-neighbour Al atoms, located in the plane perpendicular to their axis (Dederichs *et al* 1978); consequently, their configuration energy is lowered. The majority B-type configuration corresponds to a defect with an axis at the intersection of a pure Ni {100} plane with a mixed {100} plane of the lattice. These dumbbells are in a repulsive interaction with the four nearest-neighbour oversized Al atoms situated in the mixed {100} plane. The configuration energy of such B-type dumbbells is higher and depends on a balance between two opposite properties of the constituent atoms: aluminium atoms are oversized as compared to nickel atoms, while their compressibility is higher. Ni–Al mixed dumbbells are produced either on an Al site by a displaced nickel atom or on a Ni site by a displaced Al atom. In this last case, two configurations A and B, similar to the ones considered for pure Ni–Ni dumbbells, can exist.

Consideration of the different possibilities of elementary jumps of vacancies and self-interstitials shows that the easiest jump of the Ni vacancy is an exchange with a Ni atom of the Ni sublattice leading to a three-dimensional mobility in this sublattice. The most probable migration mechanism for the A-type Ni–Ni dumbbell consists of a rotation-translation jump towards a configuration of the same energy, resulting in a three-dimensional mobility on the Ni sublattice. By contrast, the migration of the less stable B-type Ni–Ni dumbbells would be a two-dimensional walk on the Ni sublattice with probably a lower activation enthalpy.

3.2.5. Interpretation of recovery stages. The first broad peak observed on the derivative

recovery curves (figure 5(*b*)) exhibits a maximum of recovery rate at $\sim$ 75 K, independent of fluence and of composition. However, its structure is complex and corresponds probably to several overlapping substages. The large amount of recovery in this stage (figure 6) suggests that ordering effects have only a minor contribution to the resistivity variations. This is further confirmed by the monotonic variation of stage I amplitude with Al content: in the case of ordering, one would expect a maximum in resistivity variation amplitude at the stoichiometric composition, as was observed during ordering induced by thermal treatments of unirradiated samples (Sitaud *et al* 1990). Therefore, by analogy with the recovery spectrum of electron-irradiated nickel, it seems reasonable to assign this stage (stage I) to the recombination of close pairs (at lower temperatures) and to the correlated and uncorrelated recombination of free Ni–Ni self-interstitials with vacancies (at higher temperatures). The temperature of stage I is somewhat higher than in pure nickel, indicating that the presence of the oversized Al atoms hinders the mobility of interstitials. By comparison with the defect recovery processes in nickel, some complexity can be attributed to the existence of Ni–Ni dumbbells with different configurations. The migration of the B-type Ni–Ni dumbbells should occur at a different temperature than that of the A-type Ni–Ni dumbbells. An alternative process would be the conversion, by *in situ* rotation, of the B-type to the A-type Ni–Ni dumbbell. Two distinct activation enthalpy values have been determined in this stage by the slope change method and lead to two distinct values: 0.16 ± 0.02 eV in the 64–77 K range (maximum recovery rate) and 0.27 ± 0.05 eV at higher temperatures (90–100 K) (Sitaud *et al* 1991). If the two Ni–Ni type dumbbells are mobile, the two activation enthalpy values could correspond either (i) to the successive migration of the two configurations of Ni–Ni dumbbells or (ii) to the recombination of the more distant close pairs (0.16 eV) followed by the migration of the more mobile Ni–Ni dumbbell on the Ni sublattice (0.28 eV). In this latter case, the migration of the second Ni–Ni dumbbell would take place at the end of stage I or in stage II.

The large decrease of the recovery amplitude in stage I with increasing Al content (figure 6) requires some discussion.

(i) The effect of constitutional vacancies cannot explain this variation. Positron lifetime and Doppler broadening measurements (Das Gupta *et al* 1985, 1987) have suggested the existence of a small concentration of constitutional vacancies in stoichiometric and hyperstoichiometric Ni_3Al ($\geqslant$ 25 at.% Al). Such vacancies should contribute to increasing the annihilation of interstitials and therefore the amplitude of stage I in the Al-rich alloy. However, the present data show the reverse evolution and are not consistent with this assumption.

(ii) Changes in the relative amplitude of resistivity recovery in stage I (table 3(*b*)) could originate from the evolution of different defect populations depending on the composition of the alloys. Recovery processes such as annihilation of specific defects or changes in the defect configuration leading to different values of the Frenkel-pair resistivity (conversion of defects, creation of antisite defects, ...) could enhance this dependence. However, these effects are not sufficient for explaining a decrease by 15% of the resistivity recovery when the Al content varies from 24.6 to 26.5 at.%.

(iii) The above comments suggest that the mechanisms of interstitial annihilation (trapping, drastic change of the mobility, ...) are strongly dependent on the Al content and that the concentration of defects is actually different at the end of stage I in the three Ni_3Al compounds.

Stage II, in the range 128–292 K, includes several substages, which can clearly

be seen as distinct peaks on the derivative curves of the hypo- and stoichiometric Ni_3Al alloys. They could correspond to the annihilation of interstitial defects of lower mobility, or to the disappearance of interstitial clusters formed in stage I.

The second large recovery stage (stage III) is observed at slightly higher temperatures (292–475 K) than in nickel: it is shifted to lower temperatures with increasing fluence (larger initial defect concentration). This stage can be reasonably assigned to the migration of vacancies, probably Ni vacancies migrating mainly on the Ni sublattice. This assignment is supported by positron lifetime measurements performed at 77 K, which detect, above 325 K, the presence of vacancy clusters formed by the aggregation of vacancies, which become mobile in this temperature range (Sitaud *et al* 1991). The main features of this stage are the following:

(i) Its amplitude is composition dependent (figure 6). It is maximum at stoichiometry similarly to the resistivity variations induced by long-range order changes in the thermally treated unirradiated samples (Sitaud *et al* 1990). This suggests that the migration of vacancies increases the long-range order of the alloys.

(ii) When the initial defect concentration becomes smaller (lower fluence), the relative amplitude of stage III increases at stoichiometry. This is consistent with a vacancy migration process: the resistivity decrease ($\Delta\rho_{ord}$) in stage III due to ordering by vacancy migration defects should be only weakly dose dependent, whereas the resistivity variations connected with defect annihilation $\Delta\rho_D^{III}$ should decrease with decreasing radiation-induced resistivity $\Delta\rho_i$. Therefore, the ratio $(\Delta\rho^{III}/\Delta\rho_i) = (\Delta\rho_{ord}^{III} + \Delta\rho_D^{III})/\Delta\rho_i$ should increase with decreasing $\Delta\rho_i$, as actually observed.

(iii) Stage III is shifted to lower temperatures with increasing Al content. This effect could be related to the existence of a larger defect concentration (larger excess resistivity) at the end of stage I in the Al-rich compound.

Activation enthalpy determinations by the slope change method, in the stoichiometric Ni_3Al, lead to a mean value $H_m^v = 1.37 \pm 0.16$ eV for vacancy migration, in the 360–425 K range, from a re-evaluation of the results of Sitaud *et al* (1991). From the temperature of the maximum recovery rates (table 3(*a*)), determined in the three alloys containing 24.6, 25.0 and 26.5 at.% Al respectively, a vacancy migration enthalpy varying from 1.38 ± 0.16 to 1.32 ± 0.16 eV can be estimated by assuming the same recovery mechanism.

A recovery stage III′, strongly dependent on composition, is observed above 475 K. From our recent positron lifetime data (Sitaud *et al* 1991) this stage does not seem to be related to the migration and annihilation of Al vacancies as previously suggested (Dimitrov *et al* 1990), but more probably to the rearrangement and dissociation of vacancy clusters. Also, the amplitude of stage III′ varies more strongly with composition than do the aluminium- and nickel-vacancy populations. The splitting of stage III′ into two substages III'_1 and III'_2 and their evolution with increasing Al content could be related to the larger defect concentration remaining at the end of stages I and III. These defects would be stabilized (trapped or converted into more stable configurations) by the increase in aluminium content up to stage III'_2, where they would dissociate or annihilate.

4. Conclusions

The recovery of low-temperature electron-irradiation damage was investigated in

Ni(Al) and Ni(Al,Ti) short-range-ordered solid solutions, and in stoichiometric and off-stoichiometric Ni_3Al long-range-ordered intermetallics.

The migration of self-interstitials does not give rise to a definite recovery stage in the Ni solid solutions; however, these defects should be mobile above 100 K, since some ordering in the binary Ni(Al) alloys is revealed by a resistivity increase. In Ni_3Al, a large recovery stage at ~ 75 K can be assigned to the elimination of Ni–Ni dumbbell interstitials. By comparison with the corresponding stage in pure nickel, which takes place around 50 K, the mobility of self-interstitials in Ni_3Al appears to be reduced by the presence of Al neighbours. Interstitial migration in Ni_3Al does not produce significant ordering effects.

Vacancy migration induces large increases of short-range order in the solid solutions; their mobility is strongly reduced in comparison with the case of pure nickel. By contrast, in the Ni_3Al intermetallics, vacancies (mainly Ni vacancies) become mobile at a temperature only slightly higher than in nickel. Their migration leads to a significant improvement of the degree of long-range order.

References

Alamo A, De Novion C H and Desarmot G 1986 *Radiat. Eff.* **88** 69–91

Bartels A, Bartusel D and Lücke K 1987a *Phys. Status Solidi* a **104** 315–28

Bartels A, Dworschak F and Weigert M 1986 *J. Nucl. Mater.* **137** 130–8

—— 1987b *J. Nucl. Mater.* **149** 160–7

Bender O and Ehrhart P 1982 *Point Defects and Defect Interactions in Metals* ed J Takamura, M Doyama and M Kiritani (Tokyo: University of Tokyo Press) pp 639–42

Caro A, Victoria M and Averback R S 1990 *J. Mater. Res.* **5** 1409–14

Das Gupta A, Smedeskjaer L C, Legnini D G and Siegel R W 1985 *Mater. Lett.* **3** 457–61

—— 1987 *Mater. Sci. Forum* **15–18** 1213–17

Dederichs P H, Lehmann C, Schober H R, Scholz A and Zeller R 1978 *J. Nucl. Mater.* **69–70** 176–99

Dimitrov C, Benkaddour A, Dimitrov O, Corbel C and Moser P 1987 *Mater. Sci. Forum* **15–18** 1275–80

Dimitrov C, Sitaud B, Zhang X, Dimitrov O, Dedek U and Dworschak F 1992 *J. Phys.: Condens. Matter* **4** 10199

Dimitrov C, Tenti M and Dimitrov O 1981 *J. Phys. F: Met. Phys.* **11** 753–65

Dimitrov C, Zhang X, Sitaud B, Dimitrov O, Dedek U and Dworschak F 1990 *Advanced Materials and Processes* ed H E Exner and V Schumacher (Oberursell: DGM) vol 1, pp 435–40

Knöll H, Dedek U and Schilling W 1974 *J. Phys. F: Met. Phys.* **4** 1095–106

Nguy T 1988 *Thesis* Université Paris-Sud

Sitaud B 1991 *Thesis* Université Paris VI

Sitaud B and Dimitrov O 1989 *Defect Diffus. Forum* **66–69** 477–82

—— 1990 *J. Phys.: Condens. Matter* **2** 7061–75

Sitaud B, Dimitrov C, Daï G, Moser P and Dimitrov O 1991 *Intermetallics Compounds* ed O Izumi (Sendai: Japan Institute of Metals) pp 69–73

Sitaud B, Zhang X, Dimitrov C and Dimitrov O 1990 *Advanced Materials and Processes* ed H E Exner and V Schumacher (Oberursell: DGM) vol 1, pp 389–94

Zhang X 1989 *Thesis* University of Caen